Materials Today Bio 32 (2025) 101650

Contents lists available at ScienceDirect

Materials Today Bio

journal homepage: www.journals.elsevier.com/materials-today-bio

Cryo-trojan mesenchymal stem cells as non-living tumor-homing supercarriers for enhanced drug delivery and immune activation in prostate cancer

Chengran Wang [1], Xinao Rong [1], Fuqiang Zhang, Xupeng Mu [*], Jinlan Jiang [**]

Department of Scientific Research Center, China-Japan Union Hospital of Jilin University, Changchun, Jilin Province, 130033, China

ARTICLE INFO

Keywords:
Prostate cancer
Mesenchymal stem cells
Drug delivery
Anthracyclines
Immunogenic cell death
Tumor microenvironment

ABSTRACT

Background: Prostate cancer remains a leading cause of cancer-related mortality, with conventional therapies limited by systemic toxicity and poor tumor targeting. Developing innovative drug delivery systems that enhance therapeutic specificity while minimizing off-target effects is critical.

Materials and methods: We engineered cryo-trojan human umbilical cord mesenchymal stem cells (CT-MSCs) as non-living, tumor-homing carriers for mitoxantrone (MTX), termed CT-MTX. Cryo-treatment preserved structural integrity and chemokine receptors (CXCR4/CCR2) for tumor targeting while eliminating proliferative risks. Comprehensive evaluations included drug loading/release kinetics, *in vitro* tumor suppression, immunogenic cell death (ICD) induction, and in vivo efficacy/safety in prostate cancer models.

Results: CT-MTX demonstrated superior drug loading (116.38 μg/10^6 cells) and pH-sensitive release (74.10 % at pH 5.5), outperforming exosomes, liposomes, and living MSCs in stability and tumor-specific drug delivery. Compared to liposomes (low targeting) and nanomaterials (biocompatibility concerns), CT-MTX leveraged MSC-derived tropism without tumorigenic risks. In vitro, CT-MTX inhibited tumor proliferation (84.83 % MTX uptake), migration (4.42 % residual migration), and induced apoptosis (43.23 % late apoptosis). Mechanistically, CT-MTX triggered ICD via PAMPs release, activating $CD8^+$ T cells and suppressing immunosuppressive Treg. In vivo, CT-MTX selectively accumulated in tumors, reducing growth by 87.88 % and extending survival (93.30 % vs. 66.70 % in controls) with negligible systemic toxicity. Proteomics revealed enriched immune pathways like NK cell cytotoxicity, validating its dual role in direct tumor killing and immune activation.

Conclusion: CT-MTX represents a novel, non-proliferative drug delivery platform that combines the tumor-homing capacity of MSCs with enhanced safety and controlled release, inducing ICDs for prostate cancer and other immunologically "cold" tumors to improve immune infiltration.

1. Introduction

Prostate cancer (PCa), one of the most frequently reported in men, leads to major reductions in the quality of life and often a poor health outlook [1]. Chemotherapy and radiotherapy are the main treatments currently used for prostate cancer; however, these treatments have limited efficacy and are associated with serious side effects, such as tissue damage and suppression of bone marrow function [2]. Through blood circulation, chemotherapy drugs reach the tumor area; however, this results in large amounts of the drug being conveyed to healthy tissues, causing harmful side effects such as nausea, hair loss, vomiting, and myelosuppression. Radiotherapy locally targets tumors but can still harm the surrounding healthy tissue, leading to radiation-induced skin problems, myelosuppression, and radiation pneumonitis [3]. Therefore, despite the role of chemotherapy and radiotherapy in prostate cancer treatment, their effectiveness and safety warrant further enhancement.

There remains an urgent need for alternative treatment methods to improve treatment outcomes and minimize unwanted effects. Researchers have focused on drug delivery systems that are more targeted and safer, optimizing drug concentration in the tumor while minimizing harm to normal tissue. These systems could improve treatment outcomes and patient quality of life [4].

* Corresponding author.
** Corresponding author.
E-mail addresses: muxupeng@jlu.edu.cn (X. Mu), jiangjinlan@jlu.edu.cn (J. Jiang).
[1] These authors contributed equally: Chengran Wang, Xinao Rong.

https://doi.org/10.1016/j.mtbio.2025.101650
Received 25 January 2025; Received in revised form 28 February 2025; Accepted 8 March 2025
Available online 12 March 2025

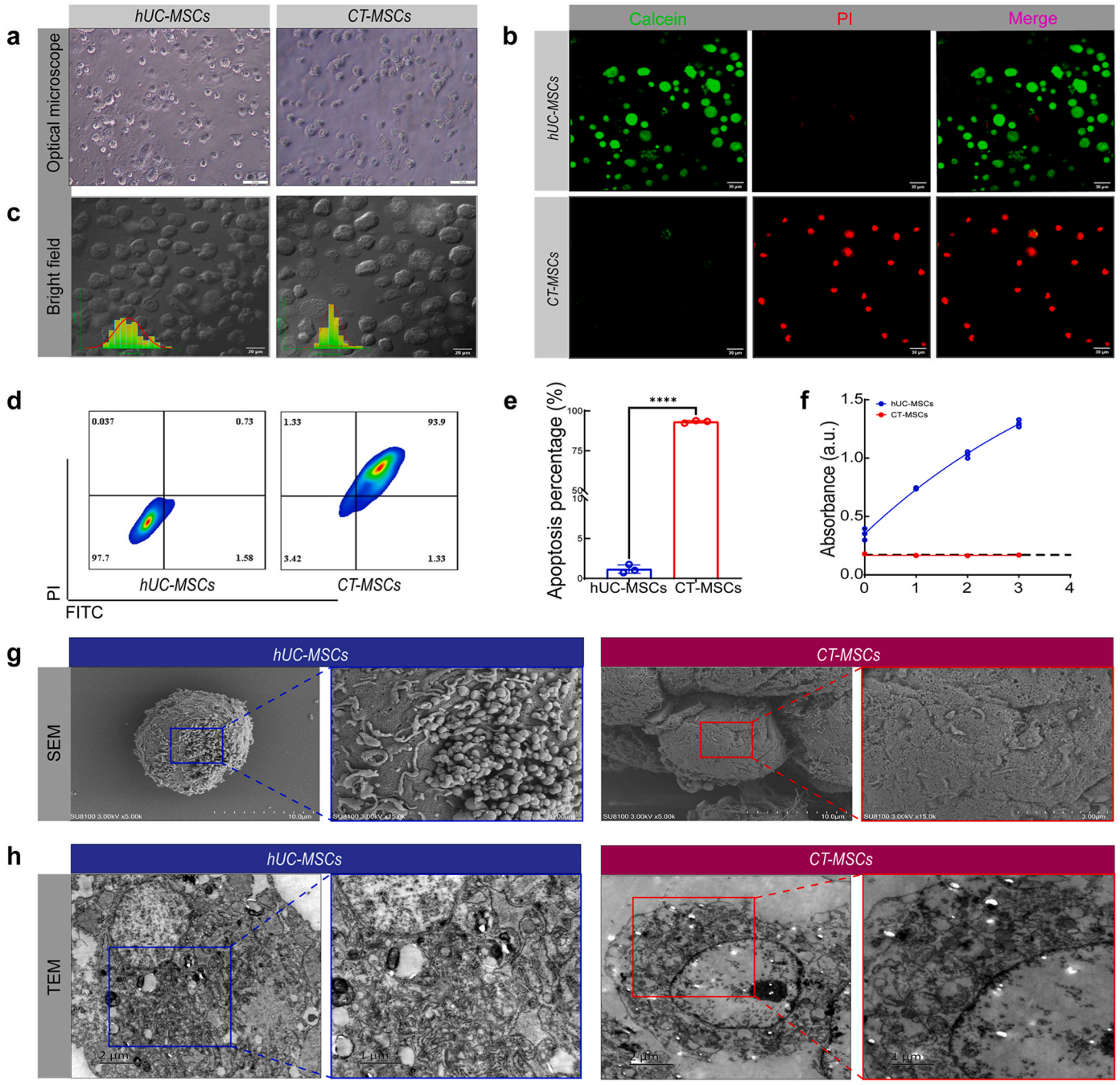

Fig. 1. Comparison of morphology, viability, apoptosis, and ultrastructure between CT-MSCs and hUC-MSCs a, Morphological characteristics of hUC-MSCs and CT-MSCs observed under optical microscopy (Scale Bar = 50 μm). **b**, Live/dead cell staining results of hUC-MSCs and CT-MSCs visualized under confocal microscopy (Scale Bar = 20 μm). **c**, Morphological characteristics of hUC-MSCs and CT-MSCs observed under confocal microscopy (Scale Bar = 30 μm). **d**, Apoptosis detection in hUC-MSCs and CT-MSCs using flow cytometry. **e**, Quantitative analysis of apoptosis data from panel d. **f**, Proliferation capacity of hUC-MSCs and CT-MSCs. **g**, Ultrastructural comparison of hUC-MSCs and CT-MSCs observed under SEM (Scale Bar = 30 μm, 10 μm). **h**, Ultrastructural comparison of hUC-MSCs and CT-MSCs observed under TEM (Scale Bar = 2 μm, 1 μm). For **e** and **f**, data were presented as means ± s.d. of n = 3 replicates (*$p < 0.05$, **$p < 0.01$, ***$p < 0.001$, ****$p < 0.0001$).

Currently, the primary drug delivery systems include exosomes, liposomes, nanomaterials, and cell delivery vehicles. Exosomes are noted for their good biocompatibility and targeting abilities [5], yet they face challenges such as complex purification, low yield, and limited drug loading capacity [6]. Liposomes are easy to produce [7]; however, they lack both targeting capabilities and stability [8]. Nanomaterials exhibit excellent properties [9–12], but their biocompatibility and potential toxicity require further investigation [13]. Cell delivery vehicles offer high drug loading, favorable biocompatibility, and precise targeting, although their clearance rates in vivo can vary significantly depending on the cell type used due to the various immunogenicity [14].

Human umbilical cord mesenchymal stem cells (hUC-MSCs) are recognized for their low immunogenicity, hence they avoid immune rejection during allogeneic transplants [15]. In addition, hUC-MSCs show high chemotaxis to tumors, enabling them to move toward and build up in the tumor environment [16], while having good compatibility with the body [17]. hUC-MSCs are a safer option than the potential tumorigenesis and uncontrolled immune response that may result from

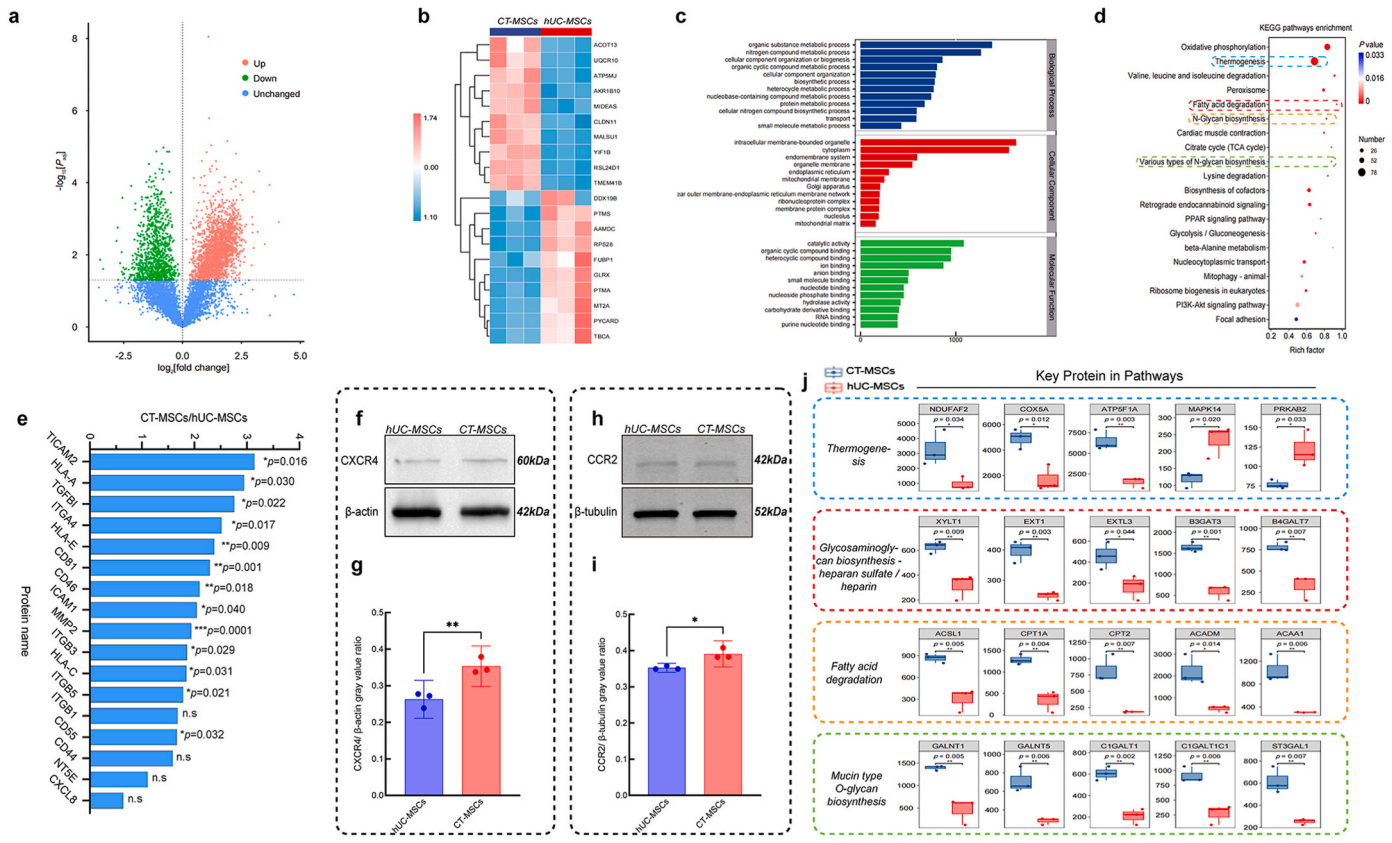

Fig. 2. Proteomic analysis and potential biological mechanisms of CT-MSCs a, Volcano plot of differentially expressed proteins between hUC-MSCs and CT-MSCs. **b**, Heatmap illustrating the clustering of differentially expressed proteins. **c**, GO analysis results. **d**, KEGG enrichment bubble plot. **e**, Expression ratios of key proteins involved in critical biological processes. **f**, Western blot analysis of CXCR4. **g**, Quantitative analysis of CXCR4 expression. **h**, Western blot analysis of CCR2. **i**, Quantitative analysis of CCR2 expression. **j**, Relative quantification of key proteins in four major pathways. For **g** and **i**, data were presented as means ± s.d. of n = 3 replicates (*$p < 0.05$, **$p < 0.01$, ***$p < 0.001$, ****$p < 0.0001$).

cryo-killed tumors or macrophages [18,19]. This makes them a suitable drug delivery system. However, living hUC-MSCs may promote tumor growth and deliver a limited amount of drugs [20]; furthermore, ethical concerns surrounding their use remain to be resolved. These issues limit their use in cancer therapy [21].

Cryo-treating is a simple and controllable method with few unwanted outcomes. Cryo-treating helps to inanimate cells while maintaining their targeting abilities and partial functions. Specifically, cryo-treating slightly damages the cell membrane and eliminates cell viability, although certain surface markers and receptors remain intact [22], helping cells to focus on tumors. Thus, cryo-trojan hUC-MSCs (CT-MSCs) behave as "non-living drug carriers" [23], delivering drugs without proliferation. Compared to living normal hUC-MSCs even to other cell-derived drug delivery systems such as leukocyte-derived or tumor-derived ones [24–26], this approach provides considerable drug loading, eliminates the risk of enhancing tumors, and avoids the ethical concerns with active stem cells, particularly in cancer treatments [27].

Additionally, cryo-treating may improve the stability of drug loading and provide controlled release. CT-MSCs create a more stable structure, allowing them to load and protect drug molecules, lowering the chance of premature release while in circulation [28]. This method provides new opportunities, particularly for anticancer drugs where targeted release is critical, ensuring that the drug functions mainly after reaching the targeted site. This can improve treatment effectiveness and reduce harm to healthy tissues. The limitations of traditional drug-loaded stem cells, such as issues with drug capacity and release control [29], have been partly improved by the cryo-treating approach, making CT-MSCs suitable for drug delivery.

This study aimed to assess the effectiveness and safety of CT-MTX for the treatment of prostate cancer. Successful use of CT-MSCs with MTX may significantly improve the treatment of prostate cancer bone metastasis while lowering systemic toxicity during therapy. This approach is important for prostate cancer treatment and other cancers, offering new methods and insights for cancer treatment in clinical settings.

2. Results

2.1. Characterization of hUC-MSCs

hUC-MSCs, abundantly present in Wharton's jelly [30,31], are possible stem cell sources. Characterization was conducted to determine whether the extracted hUC-MSCs possessed the appropriate biological properties needed for the experiments. hUC-MSCs had surface markers commonly linked with mesenchymal stem cells [32–34], such as CD73 (99.07 %, SD = 0.76 %), CD90 (99.00 %, SD = 0.26 %), and CD105 (98.75 %, SD = 0.45 %). In contrast, other markers that are not typical of MSCs [35], such as CD34, CD45, HLA-DR, CD11b, and CD19, were detected at low levels (1.20 %, SD = 0.31 %) (Supplementary Figs. 1a and b), consistent with the standard definitions of these cells. Cell growth studies (Supplementary Fig. 2) exhibited a normal growth curve, confirming their proliferative ability, and cell cycle analysis (Supplementary Figs. 3a and b) showed 73.75 % (SD = 14.92 %) of the cells in the G0/G1 phase, indicating the growth potential. The cells could differentiate into cartilage, fat, and bone, as shown by Alcian blue (Supplementary Fig. 4), Oil Red O (Supplementary Fig. 5), and Alizarin Red staining (Supplementary Fig. 6), consistent with the expected multipotency features of hUC-MSCs [35]. The overall data confirm the

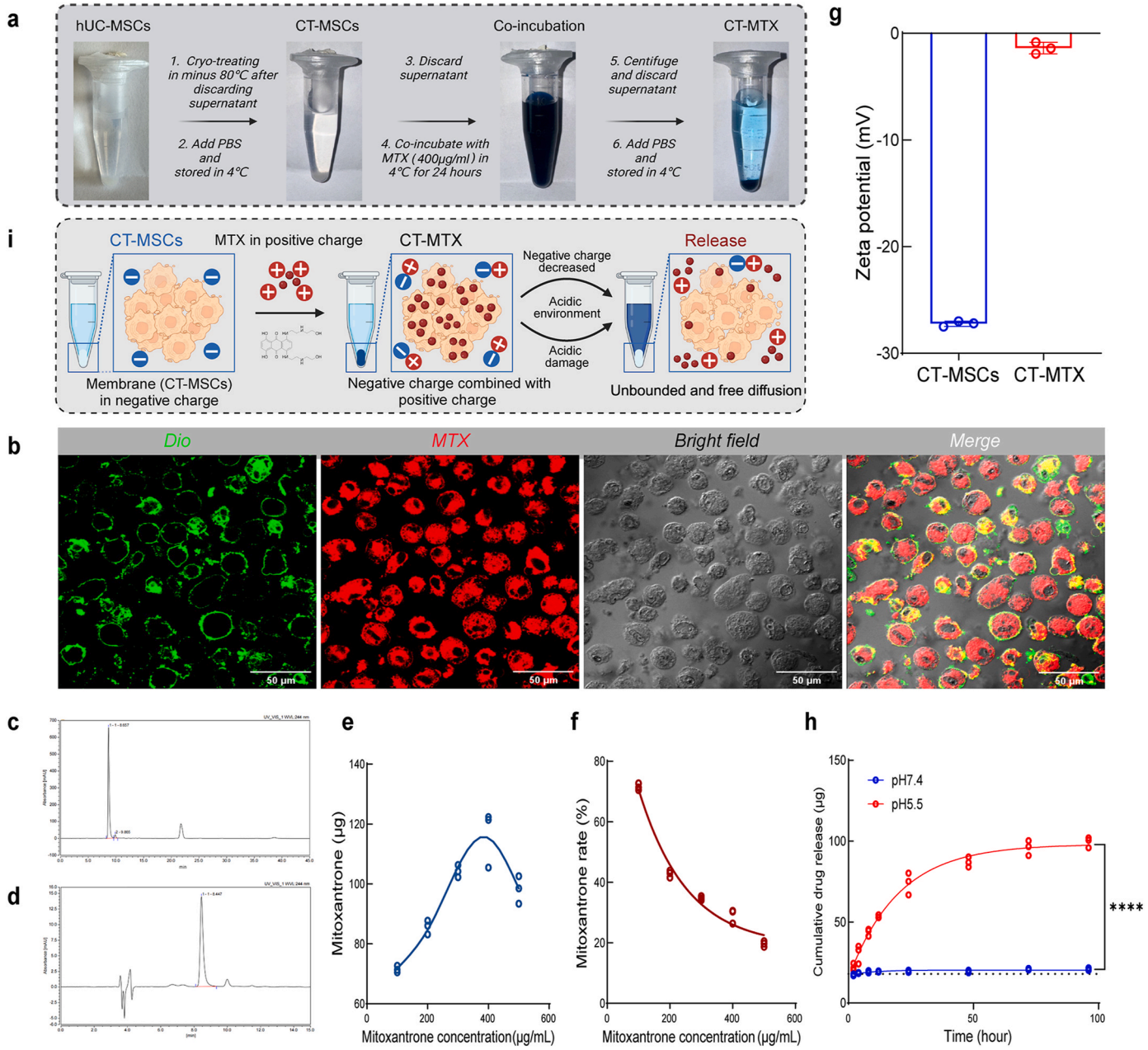

Fig. 3. Characterization of CT-MSCs as drug carriers a, Experimental outline showing CT-MTX preparation process. **b**, Staining results of CT-MTX observed under confocal microscopy (Scale Bar = 50 μm). **c**, Schematic representation of MTX content measured in CT-MSCs lysates using high-performance liquid chromatography (HPLC). **d**, Schematic representation of MTX content in the supernatant measured by HPLC during the MTX release experiment from CT-MTX. **e**, Quantitative analysis of drug loading capacity of CT-MSCs. **f**, Quantitative analysis of drug loading efficiency of CT-MSCs. **g**, Comparison of Zeta potential between CT-MSCs and CT-MTX. **h**, Time-MTX release profile of CT-MTX in different pH environments. For **e** - **h**, data were presented as means ± s.d. of n = 3 replicates (*$p < 0.05$, **$p < 0.01$, ***$p < 0.001$, ****$p < 0.0001$).

stability of the biological traits of hUC-MSCs and suggest their suitability for drug delivery carrier research.

2.2. Evaluation of cryo-treating on hUC-MSCs and their potential as drug carriers

In many cases involving cell therapy and tissue engineering, the cryopreservation of hUC-MSCs is a significant factor in preserving cell function and viability. However, for the broader use of hUC-MSCs, cryo-treating was used to determine whether CT-MSCs could retain their structure and target features, making them useful carriers for drug delivery. Compared to other methods of preparing drug delivery systems like gene engineering or chemical synthesis, the advantages of cryo-treating at −80 °C are that it is easily available, and the prepared CT-MSCs can be easily stored at −80 °C, achieving integration of preservation and preparation. Confocal microscopy using live-dead staining (Fig. 1b), trypan blue staining (Supplementary Fig. 7), and flow cytometry apoptosis analysis (Fig. 1d and e) indicated that CT-MSCs had fully lost viability, reaching necrosis and late apoptosis rates of 93.20 % (SD = 0.82 %). The growth curve also confirmed that these cells could no longer proliferate (Fig. 1f). Yet, brightfield optical and confocal microscopy images showed that CT-MSCs kept an overall intact morphology, although their diameter slightly increased (19.34 ± 3.64 μm, SD = 3.64) compared with hUC-MSCs (17.05 ± 4.79 μm, SD = 4.79) (Fig. 1a–c). Further scanning and transmission electron microscopy (Fig. 1g and h) confirmed that CT-MSCs, while biologically dead and

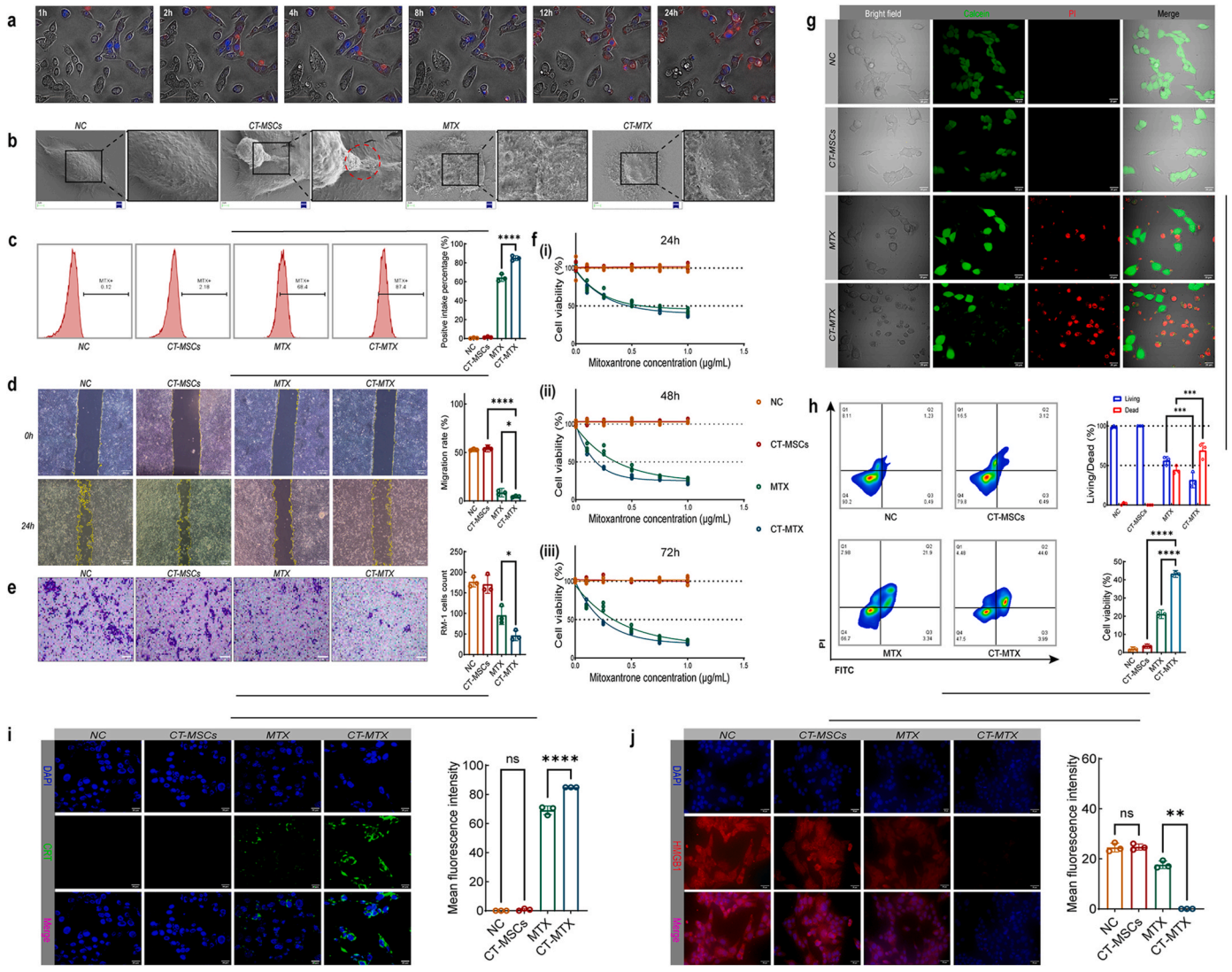

Fig. 4. Analysis of the *in vitro* targeting, tumor inhibition capability, and mechanism of CT-MTX on tumor cells a, High-content imaging shows the targeting effect of CT-MTX on RM-1 cells and the effect of MTX on tumor cells (Scale Bar = 50 μm). **b**, SEM analysis of CT-MSCs targeting RM-1 cells and the ultrastructural changes of RM-1 cells during co-culture (Scale Bar = 2 μm). **c**, Flow cytometry measurement of MTX uptake by RM-1 cells and Quantitative analysis. **d**, Scratch assay showing the migration ability of RM-1 cells in different treatment groups and quantitative analysis (Scale Bar = 200 μm). **e**, Invasion assay showing the invasive ability of RM-1 cells in different treatment groups and quantitative analysis (Scale Bar = 50 μm). **f.(i),** CCK-8 assay measuring the growth of RM-1 cells after co-culture at 24 h. **(ii),** CCK-8 assay measuring the growth of RM-1 cells after co-culture at 48 h **(iii),** CCK-8 assay measuring the growth of RM-1 cells after co-culture at 72 h **g**, Live/dead cell staining of RM-1 cells after co-culture, observed under confocal microscopy and quantitative analysis (Scale Bar = 20 μm). **h**, Flow cytometry measurement of apoptosis in RM-1 cells after co-culture and quantitative analysis. **i**, CRT expression observed under confocal microscopy and quantitative analysis (Scale Bar = 20 μm). **j**, HMGB1 expression observed under confocal microscopy and quantitative analysis (Scale Bar = 20 μm). For quantitative analysis, data were presented as means ± s.d. of n = 3 replicates (*$p < 0.05$, **$p < 0.01$, ***$p < 0.001$, ****$p < 0.0001$).

without proliferative function, retained relatively complete cellular structures without obvious destruction except their surfaces converted to be slightly rough, which might be relevant to protein changes from hUC-MSCs to CT-MSCs. These findings formed the basis for further drug loading, release, and in vivo targeting testing. While CT-MSCs lose their viability and ability to proliferate, their cellular structure, crucial for constructing drug delivery systems, remained intact.

To explore these molecular changes after cryo-treating, proteomic analysis was performed. This analysis is essential to better understand the use of CT-MSCs for drug delivery. Coomassie brilliant blue staining (Supplementary Fig. 8) showed that cryo-treating caused significant changes in the protein profiles of hUC-MSCs and CT-MSCs. The volcano plot for the differentially expressed proteins (Fig. 2a) displayed considerable protein expression shifts, whereas the heatmap analysis (Fig. 2b) illustrated the clustering of these altered proteins. The key protein expression ratio analysis (Fig. 2e) indicated that CT-MSCs responded to cryo-treating via metabolic reprogramming. Additional GO (Fig. 2c, Supplementary Fig. 9) and KEGG pathway analyses (Fig. 2d, Supplementary Fig. 10) revealed that the upregulated proteins following cryo-treating were primarily linked to oxidative phosphorylation and cell respiration. In contrast, the downregulated proteins were associated more with glycolysis and metabolite transport. Quantification of key proteins validated this pathway (Fig. 2j). These protein changes matched the structural preservation observed in the CT-MSCs, reinforcing their role as stable carriers for drug delivery. Western blot analysis (Fig. 2f–i) confirmed the upregulation of the chemokine receptors CXCR4 and CCR2 in CT-MSCs by about 34.92 % and 11.02 % [36,37], respectively, indicating that CT-MSCs might have enhanced tumor-targeting abilities.

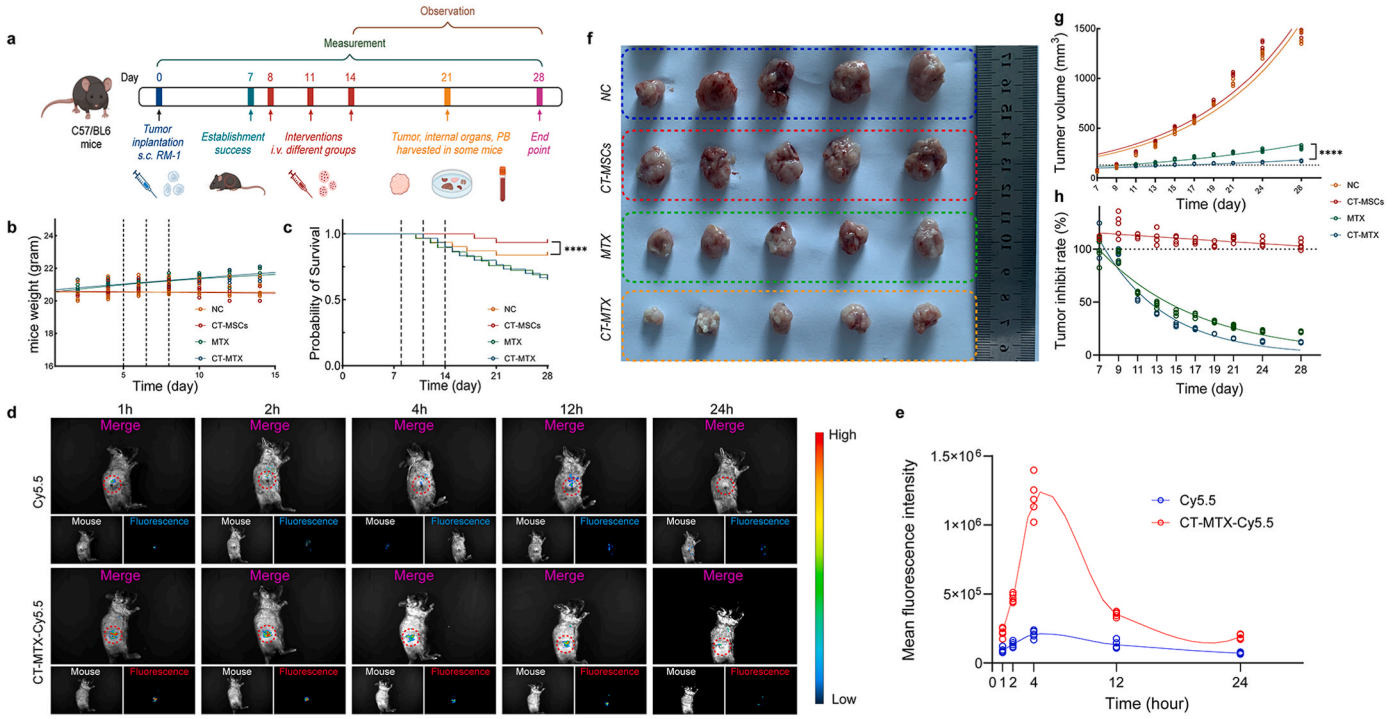

Fig. 5. Biodistribution analysis of CT-MSCs in tumor-bearing C57BL/6 mice and the antitumor efficacy of CT-MTX a, Experimental outline showing the treatment steps and procedures used to evaluate different groups in RM-1 tumor-bearing C57BL/6 mice. **b**, Changes in body weight of mice in each group. **c**, Survival curves of mice in each group. **d**, *In vivo* imaging results of tumor-bearing C57BL/6 mice. **e**, Quantitative results of fluorescence intensity at the tumor site from panel d. **f**, Tumor size in mice after different interventions. **g**, Time-dependent tumor volume curves in mice after different interventions. **h**, Time-dependent tumor inhibit rates in mice after different interventions. For quantitative results and curves, data were presented as means ± s.d. with n = 5 replicates (*$p < 0.05$, **$p < 0.01$, ***$p < 0.001$, ****$p < 0.0001$).

2.3. Drug loading, release of CT-MSCs

When studying drug delivery systems, the main consideration is how cells take drugs and release them in a controlled manner. Due to the relatively structural completeness of CT-MSCs, their drug loading and release abilities for delivery purposes were assessed. CT-MSCs (10^6) co-cultured with 1 ml MTX isotonic solution (400 μg/ml) in 4 °C for 24 h (Fig. 3a). Compared with complex operations such as exosome drug delivery (ultrasound) [38], MTX molecules are easier to enter into CT-MSCs through the small damage to the cell membrane caused by cryo-treatment, and supposed to anchor inside cytoplasm to DNA or membrane. Confocal microscopy (Fig. 3b) revealed that MTX was loaded into CT-MSCs, and high-performance liquid chromatography (Fig. 3c–e,f) proved that CT-MSCs showed high drug-loading potential and efficiency. After exposure to 400 μg/ml MTX solution, loading capacity reached about 116.38 μg/10^6 cells, while loading efficiency was approximately 29.10 %, with a superior loading capability.

To confirm the stability of CT-MTX during circulation, zeta potential measurements were conducted (Fig. 3g), converting from −27.23 ± 0.25 mV to a lower potential value (−1.38 ± 0.44 mV), which suggested that MTX with a positive charge was loaded into CT-MSCs and consequently neutralized the negative charge of the membrane (CT-MSCs), which may be one of the reasons why CT-MTX has a considerable MTX loading capacity: The attraction between opposite charges is strong, making it easy to load but not easy to release in circulation.

Notably, the drug release graphs (Fig. 3d–h) indicated that CT-MTX had a pH-sensitive controlled release in acidic conditions (pH = 5.5), where MTX release reached about 74.10 ± 6.81 μg/10^6 cells after 24 h. This observation indicates that CT-MTX shows an easier release of MTX within the acidic TME [39], just as hemoglobin tends to release oxygen more readily in environments with low oxygen levels. A more acidic environment (lower pH) typically increases positive charge [40], which may contribute to the also positively charged MTX release. In addition, a more acidic environment may cause secondary destruction of the membrane structure of CT-MTX [41], making it easier to release MTX from the broken site.

2.4. Effect of CT-MTX on the biological traits of tumor cells

To assess the potential of CT-MTX in targeting tumors, *in vitro* experiments using high-content imaging and SEM (Fig. 4a and b) revealed that CT-MTX effectively targeted RM-1 cells and caused nuclear condensation and morphological alterations. The intercellular channel between tumors and CT-MSCs has been observed using SEM (Fig. 4b). This characteristic was supposed to be used to deliver high-dose “bombs” into the tumor, effectively bypassing the tumor’s drug expulsion mechanisms. Flow cytometric analysis (Fig. 4c) confirmed that a larger proportion of RM-1 cells absorbed MTX in the CT-MTX group (84.83 ± 2.55 %) than in the MTX group (64.20 ± 3.83 %). These data underscore CT-MTX’s tumor-targeting ability of CT-MTX and support its potential role as a drug delivery platform.

Upon observing that CT-MTX could lead to changes in RM-1 cell shape, we carried out the biological characterization of these tumor cells following the intervention. The scratch test (Fig. 4d) and invasion test (Fig. 4e) showed that CT-MTX strongly reduced the migration and invasion abilities of RM-1 cells compared with the CT-MSCs and MTX groups. The migration rate was about 4.42 ± 0.69 %, and the number of invading cells was 46.00 ± 12.29. The growth curve results (Fig. 4f) showed a clear reduction in RM-1 cell growth due to CT-MTX treatment, and this effect became stronger over time. These findings show that CT-MTX plays a role in targeting tumor cells and blocking their ability to grow and move.

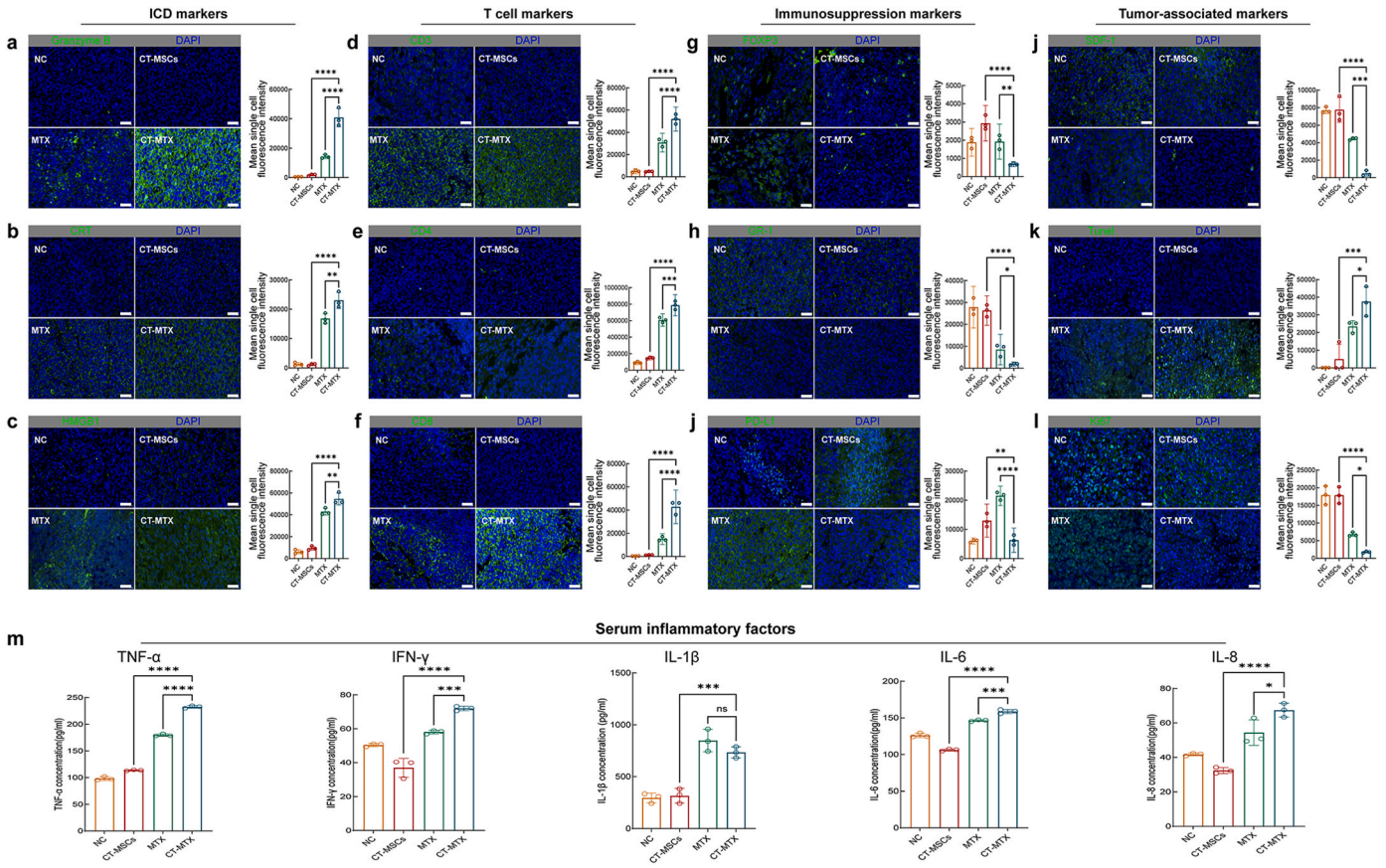

Fig. 6. Efficacy and mechanism analysis of CT-MTX in different mouse groups a, Fluorescence images showing Granzyme B staining in different treatment groups and quantitative analysis (Scale Bar = 50 μm). **b**, Fluorescence images showing CRT expression in different treatment groups and quantitative analysis (Scale Bar = 50 μm). **c**, Fluorescence images showing HMGB1 expression in different treatment groups and quantitative analysis (Scale Bar = 50 μm). **d**, Fluorescence images showing CD3 expression in different treatment groups and quantitative analysis (Scale Bar = 50 μm). **e**, Fluorescence images showing CD4 expression in different treatment groups and quantitative analysis (Scale Bar = 50 μm). **f**, Fluorescence images showing CD8 expression in different treatment groups and quantitative analysis (Scale Bar = 50 μm). **g**, Fluorescence images showing FOXP3 expression in different treatment groups and quantitative analysis (Scale Bar = 50 μm). **h**, Fluorescence images showing GR-1 expression in different treatment groups and quantitative analysis (Scale Bar = 50 μm). **i**, Fluorescence images showing PD-L1 expression in different treatment groups and quantitative analysis (Scale Bar = 50 μm). **j**, Fluorescence images showing SDF-1 expression in different treatment groups and quantitative analysis (Scale Bar = 50 μm). **k**, Fluorescence images showing TUNEL staining in different treatment groups and quantitative analysis (Scale Bar = 50 μm). **l**, Fluorescence images showing Ki67 expression in different treatment groups and quantitative analysis (Scale Bar = 50 μm). **m**, ELISA quantitative results of serum TNF-α, IFN-γ, IL-1β, IL-6, IL-8. For quantitative analysis and results, data were standardized by cell density, presented as means ± s.d. of n = 3 replicates (*$p < 0.05$, **$p < 0.01$, ***$p < 0.001$, ****$p < 0.0001$).

2.5. CT-MTX-induced immunogenic cell death

CT-MTX not only influenced the biological behavior of tumor cells but also triggered ICD in RM-1 cells, showing a different mechanism for its antitumor effects. Confocal microscopy (Fig. 4g) indicated that CT-MTX treatment substantially increased the cell death rate to 68.70 ± 9.63 %. Flow cytometry analysis (Supplementary Figs. 11a,b, Fig. 4h) demonstrated an increase in RM-1 cells in the G2 phase to 20.47 ± 1.62 %, with necrosis and late apoptosis rates reaching 43.23 ± 0.75 %. Following confirmation of RM-1 cell death, immunofluorescence analysis of CRT and HMGB1 (Fig. 4i and j) revealed a marked increase in cytoplasmic CRT levels by (23.03 ± 5.38 %) and significant decrease in cytoplasmic HMGB1, respectively, in the CT-MTX-treated group compared with the MTX group, pointing toward the role of CT-MTX in activating the host immune response through ICD induction [42,43]. However, no significance has been observed between NC and CT-MSCs groups, indicating that ICD was induced by MTX instead of CT-MSCs. These findings imply that CT-MTX not only directly influences tumor cell activity but also enhances its antitumor effects by ICD induction [44]. It is very meaningful because prostate cancers are typically known as cold cancers with low-level immune infiltration [45], by ICD, leukocytes could be recruited and activated to compose an active TME to improve those "cold" condition [46].

2.6. In vivo safety and biodistribution of CT-MSCs

To ensure the safety of CT-MSCs in vivo, their effects on organs and biodistribution were evaluated in a tumor-bearing C57BL/6 mouse model. RM-1, a prostate cancer cell line homologous to C57BL/6 mice, was used for model construction.

In vivo, fluorescence imaging (Supplementary Figs. 12a–c) displayed that CT-MSCs tagged with fluorophore Cy5.5 significantly accumulated at the tumor site. Correspondingly, the distribution of fluorescence intensity across organs (Supplementary Figs. 12c–d) in the CT-MTX-Cy5.5 group presented lower fluorescence intensities, showing that the drug delivery system could reduce the distribution of MTX in major organs, with no significant off-target effects. H&E staining (Supplementary Fig. 13) corresponds to the expected result of biodistribution: there are no significant pathological changes in the major organs following CT-MTX treatment, indicating good safety for in vivo applications.

Compared with the Cy5.5 group, the fluorescence intensity directed at tumor tissues increased by 139.69 ± 7.40 %, consistent with the *in vitro* targeting data, indicating that CT-MSCs possess strong tumor-targeting properties.

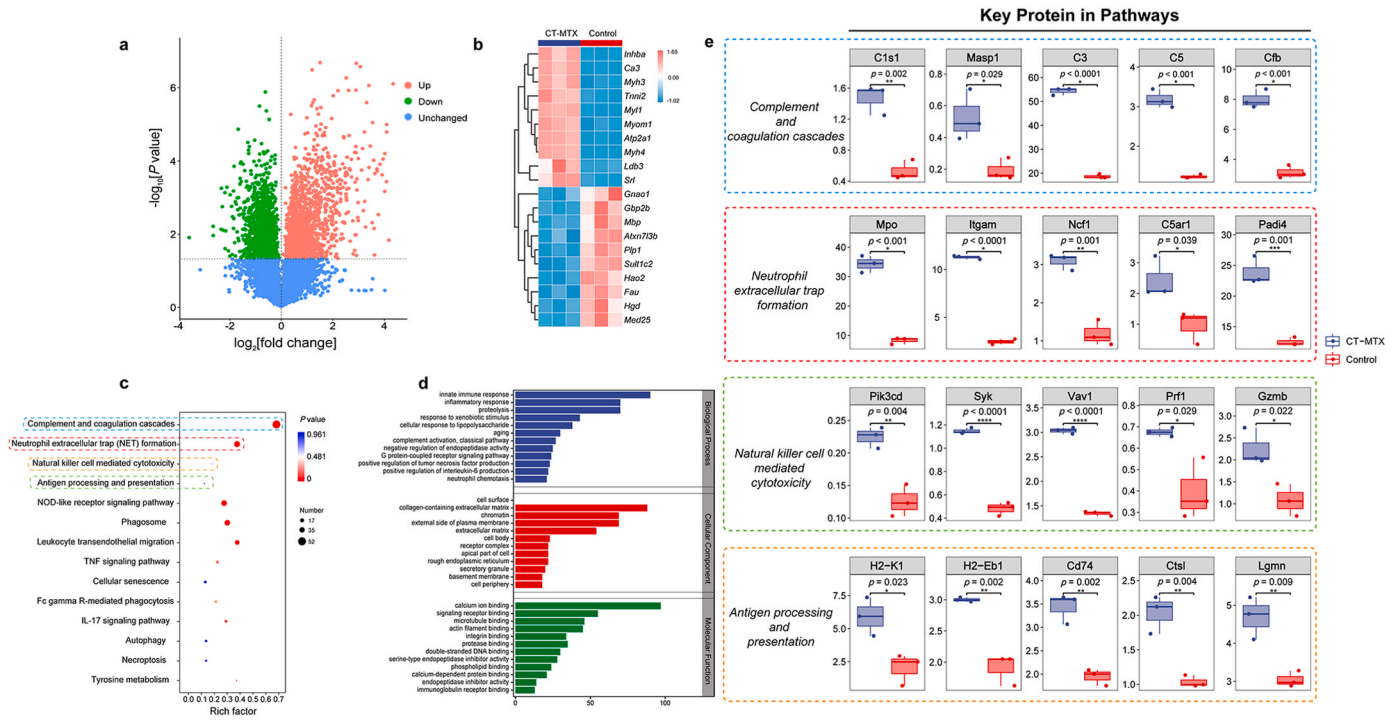

Fig. 7. The proteomic analysis of tumor tissues in CT-MTX vs. NC groups of mice. a, Volcano plot of differentially expressed genes in tumor tissues vs. NC group. **b**, A heatmap of differentially expressed genes in tumor tissues vs. NC group. **c**, KEGG enrichment analysis shows that multiple immune response and cytotoxicity-related pathways are activated, including the complement and coagulation cascade and natural killer cell-mediated cytotoxicity. **d**, GO enrichment analysis indicates that CT-MTX significantly affects several biological processes related to immune response, apoptosis, and metabolic reprogramming. **e**, Quantitative analysis of key proteins in pathways related to complement activation, NETs formation, natural killer cell-mediated cytotoxicity, and antigen processing and presentation (*$p < 0.05$, **$p < 0.01$, ***$p < 0.001$, ****$p < 0.0001$).

2.7. *In vivo* therapeutic effects of CT-MTX

After evaluating the safety and tumor-targeting capability of CT-MSCs, we next examined the therapeutic effects of CT-MTX drug-loaded carriers in treating tumors. The graph showing the tumor volume change (Fig. 5f–h) illustrates the significant role of CT-MTX in slowing tumor growth, where the tumor volume in the CT-MTX group was 56.57 ± 2.47 % of that in the MTX group, compared with the NC group, the tumor inhibition rate of CT-MTX was 87.88 ± 0.27 % after 28 days. The curve showing body weight change (Fig. 5b) suggests that CT-MTX treatment did not cause significant body weight loss, confirming low toxicity. Survival rate analysis (Fig. 5c) showed 93.30 % survival in tumor-bearing mice treated with CT-MTX on day 28 and 83.90 % in the MTX-treated group, higher than 66.70 % of NC. Mitosis in the tumor tissues of the CT-MTX group dropped to 23.27 ± 9.73 % of the MTX group (Supplementary Figs. 14a and b), showing strong tumor inhibition by CT-MTX.

The enzyme-linked immunoassay (ELISA) analysis results (Fig. 6m) revealed that pro-inflammatory cytokines, such as TNF-α, IFN-γ, IL-1β, IL-6, and IL-8, increased by 29.52 ± 2.87 %, 24.06 ± 4.60 %, 16.41 ± 21.42 %, 8.45 ± 2.36 %, and 26.06 ± 22.74 %, respectively, in the CT-MTX group compared with the MTX group. This suggests that CT-MTX improves antitumor activity by increasing inflammatory response.

2.8. *Effect of CT-MTX on migration, apoptosis, and proliferation-related markers*

Its effects on migration, apoptosis, and proliferation-related markers in tumor cells were evaluated to verify the antitumor mechanism of CT-MTX. Immunofluorescence analysis results showed that CT-MTX treatment reduced SDF-1 expression by 94.29 ± 3.80 %) compared with the MTX group (Fig. 6j), implying that CT-MTX inhibits tumor cell migration through suppression of the SDF-1-related signaling pathway [47]. TUNEL staining analysis results indicated that the CT-MTX-treated group showed an increase in TUNEL-positive signals by 123.67 ± 44.64 % compared with the MTX group (Fig. 6k), suggesting that CT-MTX induces apoptosis in tumor cells [48]. Ki67 staining results revealed that Ki67 signal intensity in the CT-MTX group decreased by 90.90 ± 1.57 % compared with the MTX group (Fig. 6l), indicating that CT-MTX reduces the proliferative capacity of tumor cells.

2.9. *Immunoanalysis of tumor microenvironment post CT-MTX treatment*

To determine how CT-MTX interacts with the immune response in the TME, we examined its impact on T-cell infiltration along with the changes seen in the main immune markers. The immunofluorescence results (Fig. 6d) showed that in the CT-MTX group, there was an 88.82 ± 29.97 % increase in $CD3^+$ T-cell fluorescence signal levels at the tumor location compared with the MTX group. Likewise, $CD4^+$ and $CD8^+$ T cell signals increased by 39.10 ± 28.80 % and 133.33 ± 21.00 %, respectively (Fig. 6e and f), indicating an increase in the CD8/CD4 ratio, which suggests a more active immune space for fighting tumors [49].

Additionally, the immunofluorescence results (Fig. 6a–c) showed that CT-MTX treatment significantly increased ICD markers, such as Granzyme B [50], CRT, and HMGB1, by 145.83 ± 15.91 times, 28.54 ± 8.33 times, and 13.83 ± 1.80 times, respectively, compared with the NC group. These findings confirm that CT-MTX strengthens specific immune responses by inducing the ICD.

There was no significant difference in ICD-related markers between the CT-MSCs group and the NC group, suggesting that the ability of CT-MTX to induce ICD originated from MTX. However, the expression levels of ICD-related and T-cell-related indexes in the CT-MTX group were higher than in the MTX group. This increase may be attributed to the

higher local concentration of CT-MTX resulting from tumor homing and the active phagocytosis of CT-MSCs by tumor cells.

After confirming that CT-MTX increased the expression of immune-related markers, we explored its effects on inhibitory immune markers in the tumor environment. The immunofluorescence analysis (Fig. 6g–i) showed that FOXP3 expression in the CT-MTX group decreased by approximately 59.82 ± 6.52 % compared with the NC group. This indicates that CT-MTX may improve antitumor immunity by reducing the buildup of Treg cells. Likewise, GR-1 signal strength decreased by 95.59 ± 1.06 %, indicating that CT-MTX lowers MDSC accumulation, thus lessening the immunosuppressive effects inside the tumor surroundings. In addition, PD-L1 expression was reduced by approximately 7.49 ± 33.18 %, indicating that CT-MTX can reduce immune evasion of tumors by reducing PD-L1.

2.10. Proteomic analysis of tumor reaction after treatment with CT-MTX

To determine how CT-MTX affects tumors, we performed a proteomic analysis. The volcano plot (Fig. 7a) showed that CT-MTX treatment altered the expression of several proteins. The heatmap results (Fig. 7b) showed how different proteins were expressed, including some linked to cytoskeletal structures, metabolism, and immune response changes.

GO and KEGG pathway analyses (Fig. 7c and d) indicated that CT-MTX-activated immune pathways, including complement and coagulation cascades and natural killer cell cytotoxicity, likely play important roles in its stronger antitumor immune response. The protein quantification results verified the activation of these immune-related pathways (Fig. 7e), supporting the assumption that CT-MTX affects tumor treatment by enhancing immune regulation.

2.11. Post-treatment safety analysis of CT-MTX

The biosafety of CT-MSCs has been considered; however, it remains essential to re-evaluate the safety of CT-MTX treatment since MTX, a chemotherapy drug, may affect several organs. H&E staining findings (Supplementary Figs. 15a–f) showed no major pathological issues, such as intramyocardial space changes in cardiac tissues, the sinusoidal region in the liver [51], germinal centers in the spleen [52], alveolar region in the lungs [53], or glomerular diameter following treatment with CT-MTX compared with the NC group [54]. This suggests favorable safety.

3. Discussion

This study represents an initial effort to use Cryo-treating MSCs as a drug delivery system, a major development in cancer treatment. In earlier studies by Gu et al. [22]. and Shi et al. [28], the use of cryo-shocked tumor cells as drug carriers were explored owing to their capacity to target tumor tissues. Moreover, there are also many other origins of drug delivery systems including immune cells [55]. However, tumor-derived carriers carry the risk of reintroducing tumorigenic materials, and unpredictable immune responses may worsen inflammation or allow immune evasion. Additionally, allogeneic immune cells may cause severe Immune rejections. Building upon the aforementioned studies on cryo-shocked cells, we have, for the first time, integrated cryopreservation techniques with human umbilical cord mesenchymal stem cells to develop a novel drug delivery system.

In contrast, CT-MSCs offer a safer alternative with fewer uncertainties. MSCs, including CT-MSCs, are not tumorigenic and naturally have low immunogenicity and strong tumor-homing abilities, which help them locate tumor sites without the risk of uncontrolled cell growth and inflammations. Additionally, CT-MSCs retain many useful properties of live MSCs, such as their ability to migrate toward inflammatory signals, meantime bridging the low-dose drug loading drawback in cell-derived drug delivery carriers, cryo-shocked tumor cells can load 65 ± 16μg/10^7 cells doxorubicin. The loading ability of living hUC-MSCs as drug carriers was 21.5 μg/10^6 cells doxorubicin loading and a loading efficiency of 3.6 % [56]. Besides, a parallel comparison to the monocyte-derived system with a taxol loading rate of 10.18 % [57]. Another research also mentioned a doxorubicin loading of neutrophils-derived system was 0.56 ± 0.04 μg/10^6 cells [58].

One of the other MSCs-derived drug delivery systems at the forefront is modified by materials science method [59–61]. Compared to them, CT-MTX achieved an ideal treatment effect at a cheaper cost.

CT-MTX has shown further improved loading capacities of cell-derived drug delivery systems, making them suitable against various benign diseases while avoiding the ethical and safety concerns associated with live stem cell treatments. Thus, CT-MSCs have achieved a balance between safety and efficacy, addressing the limitations associated with immune and tumor cells as drug carriers.

Although detailed mechanisms by which they function within the TME have been explored, several important questions remain unanswered, necessitating further research.

First, the scalability of cryo-treatment remains unvalidated. Current protocols require manual handling of MSCs, which may hinder large-scale production. Automated cryopreservation systems and standardized quality control metrics (e.g., membrane integrity post-thaw) are needed to ensure batch consistency. Second, cost-effectiveness analyses are absent Although CT-MSCs avoid the ethical and manufacturing complexities of live MSCs, the expenses associated with cryo-storage and MTX loading must be compared to synthetic carriers like liposomes, meanwhile improving cryo-treating methods to achieve more stability and mass production. This will help to address possible safety issues and expand their use in treatment.

The current sources of umbilical cord mesenchymal stem cells may present certain limitations that could hinder their large-scale application. Expanding the sources to include other genotypes could potentially address these limitations; however, further research is necessary to explore this possibility.

In addition, while the new controlled-release strategy of CT-MSCs shows great potential for improving the delivery of chemotherapeutic drugs, improvement in drug delivery and release remains essential. Furthermore, whether CT-MSCs retain these properties when exposed to different chemotherapy drugs remains to be determined.

Moreover, since its effectiveness has been observed only in prostate cancer, future research should focus on studying the effects of CT-MTX in different kinds of tumors and how it affects implication in immunotherapies, such as immune checkpoint inhibitors, for stronger combined antitumor effects. This combination could enhance the immune response, solving the issue of some immunotherapies being less effective on certain tumors or losing their efficacy over time.

Although our initial proteomic analysis showed that cryo-treating affected the molecular processes of CT-MSCs, this analysis has limitations; therefore, more research is required to understand the mechanisms underlying these effects to improve CT-MSCs further.

Finally, the primary focus of this study was validation through *in vitro* experiments and mouse models. Although these results are encouraging, extensive studies remain warranted before clinical applications. For instance, human prostate tumors often exhibit denser stroma than murine models, potentially limiting carrier penetration [62]. Addressing these limitations will be crucial for future research, the next step should be to verify the anti-tumor ability and biocompatibility of CT-MTX in patient-derived organoids or patient-derived xenotransplantation models.

In summary, this study demonstrated a new combination of the cryo-treating approach and drug delivery that targets tumors, developing CT-MTX that holds several drugs and releases them in a controlled manner, demonstrating superior antitumor effects. This study is the first to use hUC-MSCs, showing a new way to apply the cryo-treating method in cancer treatment. This new approach could lead to future cancer treatments tailored to patients. The use of CT-MSCs for carrying drugs is a safe option, providing an adaptable and predictable method for drug

delivery. This study provides other cancer treatment possibilities, advancing cancer therapy to a higher level.

4. Methods

4.1. Materials and reagents

hUC-MSCs were obtained from discarded human umbilical cords, and the RM-1 cells were obtained from Procell (China). hUC-MSCs were kept in MEMα medium (Gibco, USA) mixed with 10 % fetal bovine serum (FBS; Hyclone, USA) and 100 U/mL of penicillin and streptomycin (Biosharp, Estonia). RM-1 cells were cultured in DMEM (Gibco, USA) supplemented with 10 % FBS and 100 U/mL penicillin and streptomycin.

4.2. Sample preparation

To prepare hUC-MSCs, digestion was performed with trypsin and the cells were placed in a 15 ml centrifuge tube. The samples were centrifuged at 500 RCF for 5 min. The supernatant was discarded.

CT-MSCs preparation: hUC-MSCs were resuspended in PBS and then placed into 2-mL cryogenic vials. The cells were centrifuged at 500 RCF for 5 min, and the supernatant was discarded. The cryovials were stored at −80 °C for 24 h.

CT-MTX preparation: CT-MSCs were placed with an MTX solution of 400 μg/ml and incubated at 4 °C for 24 h. The cells were then collected via centrifugation, and the supernatant was discarded. The remaining cells were placed in PBS.

4.3. Animal experiments

The C57BL/6 mice aged 6–8 weeks were purchased from Beijing Huafukang Biological Technology Co., Ltd., China. The prostate cancer cell line RM-1, which is homologous to C57BL/6 mice, will be used for tumor model construction. The experiments involving animals for this study were approved by The Animal Experimental Ethical Inspection of the School of Public Health, Jilin University (Approval No. SY: 2024-5-005). The mice were kept under the following conditions: light/dark cycle of 12/12 h, temperature of 22 ± 1 °C, humidity between 30 % and 70 %, and free access to food and water. Each mouse was subcutaneously injected with RM-1 cells (approximately 5 × 105 cells) to create a tumor model. The mice were randomly divided into four groups. The NC (control) group received normal saline only, the CT-MSCs group was treated with CT-MSCs, the MTX group was administered MTX, and the CT-MTX group was administered CT-MTX. Dosing regimen: Doses were administered via tail-vein injection. The dosage for MTX was 6 mg/kg body weight, whereas that for CT-MSCs or CT-MTX was 6×10^7 cells per kg. Injections were administered once every 3 days, from days 8–14, for a total of three injections. The observations lasted for 14 days (days 15–28).

4.4. Cell proliferation

A CCK-8 kit (Biosharp, Tallinn, Harjumaa, Estonia) was used to evaluate cell proliferation. The assessments were performed according to the manufacturer's instructions.

4.5. Apoptosis assay

Apoptosis assay was performed to analyze cell death using an Annexin V-FITC/PI kit from Beyotime. Following the procedure described in the kit manual, the percentage of late apoptotic cells was determined using flow cytometry.

4.6. Cell cycle analysis

Cell cycle distribution was analyzed using a cell cycle assay kit (Shanghai Beyotime Bio-Technology Co., Ltd., China), following the manufacturer's instructions, and measurements were obtained using flow cytometry.

4.7. Western blotting

Western blotting was performed using specific antibodies (Proteintech Rosemont, IL, USA), according to the manufacturer's instructions. Protein extraction was performed, followed by sodium dodecyl sulfate-polyacrylamide 7.5 % gel electrophoresis separation and antibody incubation without deviation from the stated protocols.

4.8. Tissue sectioning

Tissue specimens were first fixed in 4 % paraformaldehyde for approximately one day and passed through a set of ethanol concentrations ranging from 70 % to 100 %. Next, xylene was applied twice for 1 h each time, and the samples were placed in hot paraffin. Once the paraffin cooled and solidified, the blocks were cut into thin slices, 4–6 μm thick, using a microtome and prepared for further steps.

4.9. Immunofluorescence staining

The immunofluorescence staining was performed using antibodies and dyes (Proteintech Rosemont, IL, USA) following the manufacturer's instructions. Sample fixation, antibody steps, and dye application were performed according to the manufacturer's instructions, and images were captured using a confocal microscope.

4.10. In vivo imaging

Cy5.5 dye (Shanghai Yuanye Bio-Technology Co., Ltd., China) was administered to mice at a dose of 50 μg per mouse, and imaging with an in vivo system was carried out, enabling observation of how drugs might be spread in the body. Three channels were saved from IVIS: mouse, fluorescence, and merge, where the fluorescence channels were quantified using ImageJ software. The thresholds of Cy5.5 group and CT-MTX-Cy5.5 group were consistent.

4.11. ELISA assay

ELISA tests were performed using kits (Cohesion Biosciences, London, UK), following the manufacturer's instructions, to detect the levels of specific proteins or cytokines present within the samples being analyzed.

4.12. Statistical analysis

GraphPad Prism 9 and Origin software were used to examine the experimental data. Comparisons between groups were performed using t-tests or one-way analysis of variance. In multiple comparisons, Tukey's post hoc test was used. Fluorescent sections, and in vivo imaging were analyzed using image j, for mean fluorescence intensity analysis, the fluorescence intensity was normalized using cell density. Flow cytometry analysis was performed using Flowjo 10. $^*p < 0.05$, $^{**}p < 0.01$, $^{***}p < 0.001$, $^{****}p < 0.0001$ was considered statistically significant.

CRediT authorship contribution statement

Chengran Wang: Writing – original draft, Methodology, Conceptualization. **Xinao Rong:** Writing – review & editing, Visualization, Methodology, Formal analysis, Data curation. **Fuqiang Zhang:** Writing – review & editing. **Xupeng Mu:** Writing – review & editing,

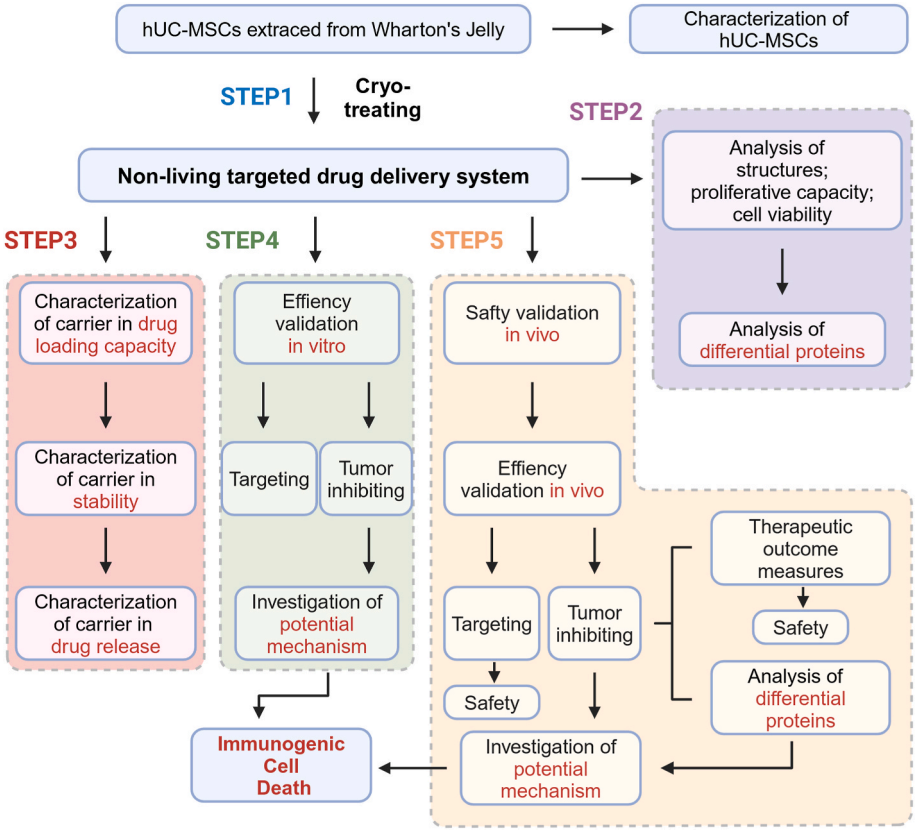

Supervision, Conceptualization. **Jinlan Jiang:** Supervision, Resources, Funding acquisition.

Ethics and consent to participate declarations

The experiments involving animals for this study complied with the ARRIVE guidelines and were approved by The Animal Experimental Ethical Inspection of the School of Public Health, Jilin University (Approval No. SY: 2024-5-005).

Workflow

The overall workflow outlines the study to help readers understand the experimental design.

Declaration of competing interest

The authors declare that they have no known competing financial interests or personal relationships that could have appeared to influence the work reported in this paper.

Acknowledgments

The authors acknowledge fundings from the National Natural Science Foundation of China (Grant No. 82172230), and the Jilin Scientific and Technological Development Program (Grant No. 20240205001YY).

Appendix A. Supplementary data

Supplementary data to this article can be found online at https://doi.org/10.1016/j.mtbio.2025.101650.

Data availability

Data will be made available on request.

References

[1] N. Chen, C.R. Hu, H.S. Iyer, P. James, B.A. Dickerman, L.A. Mucci, R.C. Nethery, Neighborhood greenness and long-term physical and psychosocial quality of life among prostate cancer survivors in the Health Professionals Follow-up Study, Environ. Res. (2024) 119847, https://doi.org/10.1016/j.envres.2024.119847.
[2] M.R. Fattahi, M. Dehghani, S. Paknahad, S. Rahiminia, D. Zareie, B. Hoseini, T. R. Oroomi, H. Motedayyen, R. Arefnezhad, Clinical insights into nanomedicine and biosafety: advanced therapeutic approaches for common urological cancers, Front. Oncol. 14 (2024) 1438297, https://doi.org/10.3389/fonc.2024.1438297.
[3] D. Özistanbullu, R. Weber, M. Schröder, S. Kippenberger, J. Kleemann, H. Stege, R. Kaufmann, B. Schilling, S. Grabbe, R. Wilhelm, Exploring the thoughts, needs and fears of chemotherapy patients—an analysis based on google search behavior, Healthcare 12 (2024) 1689, https://doi.org/10.3390/healthcare12171689.
[4] L. Sun, H. Liu, Y. Ye, Y. Lei, R. Islam, S. Tan, R. Tong, Y.-B. Miao, L. Cai, Smart nanoparticles for cancer therapy, Signal Transduct. Targeted Ther. 8 (2023) 418, https://doi.org/10.1038/s41392-023-01642-x.
[5] M.-H. Chan, Z.-X. Chang, C.-Y.F. Huang, L.J. Lee, R.-S. Liu, M. Hsiao, Integrated therapy platform of exosomal system: hybrid inorganic/organic nanoparticles with exosomes for cancer treatment, Nanoscale Horiz 7 (2022) 352–367, https://doi.org/10.1039/D1NH00637A.
[6] V. Poinsot, N. Pizzinat, V. Ong-Meang, Engineered and mimicked extracellular nanovesicles for therapeutic delivery, Nanomaterials 14 (2024) 639, https://doi.org/10.3390/nano14070639.
[7] J. Kim, C. Gao, P. Guo, J. Sheng, J. Wang, A novel approach to alleviate acetaminophen-induced hepatotoxicity with hybrid balloon flower root-derived exosome-like nanoparticles (BDEs) with silymarin via inhibition of hepatocyte MAPK pathway and apoptosis, Cell Commun. Signal. 22 (2024) 334, https://doi.org/10.1186/s12964-024-01700-z.
[8] M.J.W. Evers, S.I. van de Wakker, E.M. de Groot, O.G. de Jong, J.J.J. Gitz-François, C.S. Seinen, J.P.G. Sluijter, R.M. Schiffelers, P. Vader, Functional siRNA delivery by extracellular vesicle–liposome hybrid nanoparticles, Adv. Healthcare Mater. 11 (2022) 2101202, https://doi.org/10.1002/adhm.202101202.
[9] Department of Physiology, Faculty of Medical Sciences, University of Kragujevac, Serbia, G. Rosic, Cancer signaling, cell/gene therapy, diagnosis and role of nanobiomaterials, ABES 9 (2024) 11–34, https://doi.org/10.62476/abes9s11.

[10] Institute of Radiation Problems, Ministry of Science and Education, Azerbaijan Baku, A. Nasibova, The modern perspectives of nanomaterial applications in cancer treatment and drug delivery, ABES 9 (2024) 330–337, https://doi.org/10.62476/abes93330.
[11] Department of Biophysics and Biochemistry, Faculty of Biology, Baku State University, Azerbaijan Baku, R. Khalilov, Interactions of nanoparticles and biological systems, ABES 9 (2024) 311–318, https://doi.org/10.62476/abes93311.
[12] S. Montazersaheb, A. Eftekhari, A. Shafaroodi, S. Tavakoli, S. Jafari, A. Baran, M. F. Baran, S. Jafari, E. Ahmadian, Green-synthesized silver nanoparticles from peel extract of pumpkin as a potent radiosensitizer against triple-negative breast cancer (TNBC), Cancer Nanotechnology 15 (2024) 47, https://doi.org/10.1186/s12645-024-00285-z.
[13] J. Wang, X. Zhang, J. Xing, L. Gao, H. Lu, Nanomedicines in diagnosis and treatment of prostate cancers: an updated review, Front. Bioeng. Biotechnol. 12 (2024), https://doi.org/10.3389/fbioe.2024.1444201.
[14] A. Kostyusheva, S. Brezgin, N. Ponomareva, A. Frolova, A. Lunin, E. Bayurova, A. Tikhonov, O. Slatinskaya, P. Demina, A. Kachanov, G. Babayeva, I. Khan, D. Khochenkov, Y. Khochenkova, D. Sokolova, D. Silachev, G. Maksimov, E. Khaydukov, V.S. Pokrovsky, A.A. Zamyatnin, A. Parodi, I. Gordeychuk, V. Chulanov, D. Kostyushev, Biologics-based technologies for highly efficient and targeted RNA delivery, Mol. Ther. 33 (2025) 168–183, https://doi.org/10.1016/j.ymthe.2024.11.004.
[15] S. Meshitsuka, R. Ninomiya, T. Nagamura-Inoue, T. Okada, M. Futami, A. Tojo, CRISPR/Cas9 and AAV mediated insertion of β2 microglobulin-HLA-G fusion gene protects mesenchymal stromal cells from allogeneic rejection and potentiates the use for off-the-shelf cell therapy, Regen Ther 21 (2022) 442–452, https://doi.org/10.1016/j.reth.2022.09.009.
[16] S.S. Chetty, S. Praneetha, A. Vadivel Murugan, K. Govarthanan, R.S. Verma, Human umbilical cord Wharton's jelly-derived mesenchymal stem cells labeled with Mn^{2+} and Gd^{3+} Co-doped $CuInS_2$ –ZnS nanocrystals for multimodality imaging in a tumor mice model, ACS Appl. Mater. Interfaces 12 (2020) 3415–3429, https://doi.org/10.1021/acsami.9b19054.
[17] I.A. Deus, J.F. Mano, C.A. Custódio, Perinatal Tissues and Cells in Tissue Engineering and Regenerative Medicine, (n.d.).
[18] Z. Zhu, X. Zhang, X. Lin, Y. Wang, C. Han, S. Wang, Research advances and application progress on miRNAs in exosomes derived from M2 macrophage for tissue injury repairing, IJN 20 (2025) 1543–1560, https://doi.org/10.2147/IJN.S508781.
[19] Y. Yang, T. Ye, F. Shang, D. Chen, K. Wang, S. He, Combined albumin polyester nanocarriers with docetaxel for effective against lung cancer in mice model, IJN 20 (2025) 2103–2118, https://doi.org/10.2147/IJN.S487344.
[20] L. Dong, Y. Pu, L. Zhang, Q. Qi, L. Xu, W. Li, C. Wei, X. Wang, S. Zhou, J. Zhu, X. Wang, F. Liu, X. Chen, C. Su, Human umbilical cord mesenchymal stem cell-derived extracellular vesicles promote lung adenocarcinoma growth by transferring miR-410, Cell Death Dis. 9 (2018) 218, https://doi.org/10.1038/s41419-018-0323-5.
[21] N.M. King, J. Perrin, Ethical issues in stem cell research and therapy, Stem Cell Res. Ther. 5 (2014) 85, https://doi.org/10.1186/scrt474.
[22] T. Ci, H. Li, G. Chen, Z. Wang, J. Wang, P. Abdou, Y. Tu, G. Dotti, Z. Gu, Cryo-shocked cancer cells for targeted drug delivery and vaccination, Sci. Adv. 6 (2020), https://doi.org/10.1126/sciadv.abc3013 eabc3013.
[23] Z. Zhao, L. Fang, P. Xiao, X. Sun, L. Zhou, X. Liu, J. Wang, G. Wang, H. Cao, P. Zhang, Y. Jiang, D. Wang, Y. Li, Walking dead tumor cells for targeted drug delivery against lung metastasis of triple-negative breast cancer, Adv. Mater. 34 (2022) 2205462, https://doi.org/10.1002/adma.202205462.
[24] Y.-Y. Lin, Cell-derived Artificial Nanovesicle as a Drug Delivery System for Malignant Melanoma Treatment, 2022.
[25] L. Tang, S. He, Y. Yin, H. Liu, J. Hu, J. Cheng, W. Wang, Combination of Nanomaterials in Cell-Based Drug Delivery Systems for Cancer Treatment, 2021.
[26] W. Zhao, K. Li, L. Li, R. Wang, Y. Lei, H. Yang, L. Sun, Mesenchymal stem cell-derived exosomes as drug delivery vehicles in disease therapy, IJMS 25 (2024) 7715, https://doi.org/10.3390/ijms25147715.
[27] X. Yang, Z. Li, Y. Ma, J. Gao, S. Liu, Y. Gao, G. Wang, Human umbilical cord mesenchymal stem cells promote carcinoma growth and lymph node metastasis when co-injected with esophageal carcinoma cells in nude mice, Cancer Cell Int. 14 (2014) 93, https://doi.org/10.1186/s12935-014-0093-9.
[28] Q. Wu, H. Huang, M. Sun, R. Zhang, J. Wang, H. Zheng, C. Zhu, S. Yang, X. Shen, J. Shi, F. Liu, W. Wu, J. Sun, F. Liu, H. Li, Z. Gu, Inhibition of tumor metastasis by liquid-nitrogen-shocked tumor cells with oncolytic viruses infection, Adv. Mater. 35 (2023) 2212210, https://doi.org/10.1002/adma.202212210.
[29] L. Xie, C. Zhang, M. Liu, J. Huang, X. Jin, C. Zhu, M. Lv, N. Yang, S. Chen, M. Shao, X. Du, G. Feng, Nucleus-targeting manganese dioxide nanoparticles coated with the human umbilical cord mesenchymal stem cell membrane for cancer cell therapy, ACS Appl. Mater. Interfaces 15 (2023) 10541–10553, https://doi.org/10.1021/acsami.3c01176.
[30] K. Stefańska, L. Nemcova, M. Blatkiewicz, A. Żok, M. Kaczmarek, W. Pieńkowski, P. Mozdziak, H. Piotrowska-Kempisty, B. Kempisty, Expression profile of new marker genes involved in differentiation of human Wharton's jelly-derived mesenchymal stem cells into chondrocytes, Osteoblasts, Adipocytes and Neural-like Cells, IJMS 24 (2023) 12939, https://doi.org/10.3390/ijms241612939.
[31] H. Yang, Y. Zhou, Y. Bi, X. Dong, Q. Qian, S. Gao, Effects of human umbilical cord mesenchymal stem cell-derived exosomes in the rat osteoarthritis models, Stem Cells Transl Med 13 (2024) 803–811, https://doi.org/10.1093/stcltm/szae031.
[32] F. Liu, Long Non-coding RNA CIR Inhibits Chondrogenic Differentiation of Mesenchymal Stem Cells by Epigenetically Suppressing ATOH8 via Methyltransferase EZH2, 2021.
[33] X. Zhou, J. Gu, Y. Gu, M. He, Y. Bi, J. Chen, T. Li, Human umbilical cord-derived mesenchymal stem cells improve learning and memory function in hypoxic-ischemic brain-damaged rats via an IL-8. Mediated Secretion Mechanism rather than Differentiation Pattern Induction, 2015.
[34] N. Hendrijantini, P. Hartono, Phenotype characteristics and osteogenic differentiation potential of human mesenchymal stem cells derived from amnion membrane (HAMSCs) and umbilical cord (HUC-MSCs), Acta Inf. Med. 27 (2019) 72, https://doi.org/10.5455/aim.2019.27.72-77.
[35] S. Maslennikov, G. Maksym, The Most Commonly Used Cell Surface Markers for Determining Mesenchymal Stromal Cells in Stromal Vascular Fraction and Bone Marrow Autologous Concentrate: a Systematic Review, (n.d.).
[36] X.-H. Ren, X.-Y. He, C. Xu, D. Han, S.-X. Cheng, Functional tumor targeting nano-systems for reprogramming circulating tumor cells with in situ evaluation on therapeutic efficiency at the single-cell level, Adv. Sci. (Weinh) 9 (2022) e2105806, https://doi.org/10.1002/advs.202105806.
[37] M.W. Oo, H. Kawai, K. Takabatake, S. Tomida, T. Eguchi, K. Ono, Q. Shan, T. Ohara, S. Yoshida, H. Omori, S. Sukegawa, K. Nakano, K. Okamoto, A. Sasaki, H. Nagatsuka, Resident stroma-secreted chemokine CCL2 governs myeloid-derived suppressor cells in the tumor microenvironment, JCI Insight 7 (2022) e148960, https://doi.org/10.1172/jci.insight.148960.
[38] Y.-J. Li, J.-Y. Wu, J. Liu, W. Xu, X. Qiu, S. Huang, X.-B. Hu, D.-X. Xiang, Artificial exosomes for translational nanomedicine, J. Nanobiotechnol. 19 (2021) 242, https://doi.org/10.1186/s12951-021-00986-2.
[39] Z. Li, W. Zhao, N. Liang, P. Yan, S. Sun, Tumor targeting and pH-sensitive inclusion complex based on HP-β-CD as a potential carrier for paclitaxel: fabrication, molecular docking, and characterization, Biomacromolecules 24 (2023) 178–189, https://doi.org/10.1021/acs.biomac.2c01023.
[40] A.A.R. Pereira, J.V.M. Aparecida, M.E. Ramalho, L.M.B. Ferreira, M.P.D. Gremião, Tailoring mesalazine nanosuspension using chitosan polyelectrolyte complexes with alginate and alginate/hydroxypropyl-methylcellulose phthalate, Pharmaceutics 16 (2024) 1489, https://doi.org/10.3390/pharmaceutics16121489.
[41] M. Tavakoli, S. Maghsoudian, A. Rezaei-Aderiani, M. Hajiramezanali, Y. Fatahi, M. Amani, E. Sharifikolouei, M.H. Ghahremani, M. Raoufi, H. Motasadizadeh, R. Dinarvand, Synergistic effects of paclitaxel and platelet-superparamagnetic iron oxide nanoparticles for targeted chemo-hyperthermia therapy against breast cancer, Colloids Surf. B Biointerfaces 251 (2025) 114584, https://doi.org/10.1016/j.colsurfb.2025.114584.
[42] L.-P. Zhao, R.-R. Zheng, X.-N. Rao, C.-Y. Huang, H.-Y. Zhou, X.-Y. Yu, X.-Y. Jiang, S.-Y. Li, Chemotherapy-enabled colorectal cancer immunotherapy of self-delivery nano-PROTACs by inhibiting tumor glycolysis and avoiding adaptive immune resistance, Adv. Sci. (Weinh) 11 (2024) e2309204, https://doi.org/10.1002/advs.202309204.
[43] J. Fucikova, Detection of Immunogenic Cell Death and its Relevance for Cancer Therapy, 2020.
[44] G.-Q. Xia, T.-R. Lei, T.-B. Yu, P.-H. Zhou, Nanocarrier-based activation of necroptotic cell death potentiates cancer immunotherapy, Nanoscale 13 (2021) 1220–1230, https://doi.org/10.1039/D0NR05832G.
[45] L. Brea, J. Yu, Tumor-intrinsic regulators of the immune-cold microenvironment of prostate cancer, Trends Endocrinol. Metabol. 0 (2025), https://doi.org/10.1016/j.tem.2024.12.003.
[46] C. Wu, D. Feng, H. Xu, Z. He, J. Hou, Optimized bionic drug-delivery-inducing immunogenic cell death and cGAS-STING pathway activation for enhanced photodynamic-chemotherapy-driven immunotherapy in prostate cancer, ACS Appl. Mater. Interfaces 16 (2024) 43257–43271, https://doi.org/10.1021/acsami.4c07072.
[47] B.A. Teicher, S.P. Fricker, CXCL12 (SDF-1)/CXCR4 pathway in cancer, Clin. Cancer Res. 16 (2010) 2927–2931, https://doi.org/10.1158/1078-0432.CCR-09-2329.
[48] R. Mirzayans, D. Murray, Do TUNEL and other apoptosis assays detect cell death in preclinical studies? IJMS 21 (2020) 9090, https://doi.org/10.3390/ijms21239090.
[49] M.A. Cerqueira, K.L. Ferrari, A.C. de Mattos, C.R. Monti, L.O. Reis, T cells CD4+/CD8+ local immune modulation by prostate cancer hemi-cryoablation, World J. Urol. 38 (2020) 673–680, https://doi.org/10.1007/s00345-019-02861-0.
[50] A. Valančiūtė, L. Mathieson, R.A. O'Connor, J.I. Scott, M. Vendrell, D.A. Dorward, A.R. Akram, K. Dhaliwal, Phototherapeutic Induction of Immunogenic Cell Death and CD8+ T Cell-Granzyme B Mediated Cytolysis in Human Lung Cancer Cells and Organoids, 2022.
[51] D.P. van Asseldonk, M. Simsek, E. Bloemena, M.G. Russel, B.I. Lissenberg-Witte, C. M. van Nieuwkerk, J. Mulder, J. Verheij, A.A. van Bodegraven, Limited Relevance and Progression of Histological Alterations in the Liver during Thioguanine Therap, (n.d.).
[52] J. Schwenck, B. Schörg, F. Fiz, D. Sonanini, A. Forschner, T. Eigentler, B. Weide, M. Martella, I. Gonzalez-Menendez, C. Campi, G. Sambuceti, F. Seith, L. Quintanilla-Martinez, C. Garbe, C. Pfannenberg, M. Röcken, C.L. Fougere, B. J. Pichler, M. Kneilling, Cancer immunotherapy is accompanied by distinct metabolic patterns in primary and secondary lymphoid organs observed by non-invasive *in vivo* 18 F-FDG-PET, Theranostics 10 (2020) 925–937, https://doi.org/10.7150/thno.35989.
[53] G. Matute-Bello, G. Downey, B.B. Moore, S.D. Groshong, M.A. Matthay, A. S. Slutsky, W.M. Kuebler, An official American thoracic society workshop report: features and measurements of experimental acute lung injury in animals, Am. J. Respir. Cell Mol. Biol. 44 (2011) 725–738, https://doi.org/10.1165/rcmb.2009-0210ST.
[54] A. Kato, A. Hishida, S. Kobayashi, N. Honda, Glomerular alterations in experimental oliguric and nonoliguric acute renal failure, Ren. Fail. 15 (1993) 215–224, https://doi.org/10.3109/08860229309046155.

[55] F. Combes, E. Meyer, N.N. Sanders, Immune cells as tumor drug delivery vehicles, J. Contr. Release 327 (2020) 70–87, https://doi.org/10.1016/j.jconrel.2020.07.043.
[56] Y. Takayama, K. Kusamori, C. Tsukimori, Y. Shimizu, M. Hayashi, I. Kiyama, H. Katsumi, T. Sakane, A. Yamamoto, M. Nishikawa, Anticancer drug-loaded mesenchymal stem cells for targeted cancer therapy, J. Contr. Release 329 (2021) 1090–1101, https://doi.org/10.1016/j.jconrel.2020.10.037.
[57] T. Lang, X. Dong, Y. Huang, W. Ran, Q. Yin, P. Zhang, Z. Zhang, H. Yu, Y. Li, Ly6C^{hi} monocytes delivering pH-sensitive micelle loading paclitaxel improve targeting therapy of metastatic breast cancer, Adv. Funct. Mater. 29 (2019) 1904596, https://doi.org/10.1002/adfm.201904596.
[58] J. Ding, D. Sui, M. Liu, Y. Su, Y. Wang, M. Liu, X. Luo, X. Liu, Y. Deng, Y. Song, Sialic acid conjugate-modified liposomes enable tumor homing of epirubicin via neutrophil/monocyte infiltration for tumor therapy, Acta Biomater. 134 (2021) 702–715, https://doi.org/10.1016/j.actbio.2021.07.063.
[59] Y. Yu, Y. Tao, J. Ma, J. Li, Z. Song, Targeting the tumor microenvironment with mesenchymal stem cells based delivery approach for efficient delivery of anticancer agents: an updated review, Biochem. Pharmacol. 232 (2025) 116725, https://doi.org/10.1016/j.bcp.2024.116725.
[60] Y. Matsuzaka, R. Yashiro, Current strategies and therapeutic applications of mesenchymal stem cell-based drug delivery, Pharmaceuticals 17 (2024) 707, https://doi.org/10.3390/ph17060707.
[61] Y. Xiao, R.-H. Xu, Y. Dai, Nanoghosts: harnessing mesenchymal stem cell membrane for construction of drug delivery platforms via optimized biomimetics, Small 20 (2024) 2304824, https://doi.org/10.1002/smll.202304824.
[62] M. Bogaard, R.I. Skotheim, A.V. Maltau, S.G. Kidd, R.A. Lothe, K. Axcrona, U. Axcrona, 'High proliferative cribriform prostate cancer' defines a patient subgroup with an inferior prognosis, Histopathology 83 (2023) 853–869, https://doi.org/10.1111/his.15012.